International Journal of Heat and Mass Transfer 108 (2017) 2355–2364

Contents lists available at ScienceDirect

International Journal of Heat and Mass Transfer

journal homepage: www.elsevier.com/locate/ijhmt

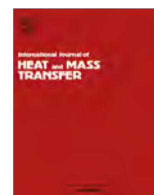

Global simulation of coupled oxygen and carbon transport in an industrial directional solidification furnace for crystalline silicon ingots: Effect of crucible cover coating

Lijun Liu [a,*], Wencheng Ma [a], Xiaofang Qi [a], Zaoyang Li [a], Yunfeng Zhang [b]

[a] Key Laboratory of Thermo-Fluid Science and Engineering, Ministry of Education, School of Energy and Power Engineering, Xi'an Jiaotong University, Xi'an, Shaanxi 710049, China
[b] Yingli Green Energy Holding Co. Ltd., Baoding, Hebei 071051, China

ARTICLE INFO

Article history:
Received 13 October 2016
Received in revised form 23 January 2017
Accepted 23 January 2017

Keywords:
Transient global simulation
Oxygen and carbon transport
Impurity segregation
Directional solidification
Silicon

ABSTRACT

For accurate prediction of oxygen (O) and carbon (C) distributions in the crystalline silicon ingots grown by the industrial directional solidification (DS) furnace, we first performed transient global simulations of heat transfer based on a fully coupled calculation of the thermal and flow fields. The phase change problem was handled by an enthalpy formulation technique based on a fixed-grid methodology. The coupled C and O transport in the DS furnace was then carried out, taking into account five chemical reactions. Special attention was devoted to modeling the O and C impurity segregation during the entire solidification process. It was found that the developed model can successfully simulate the impurity segregation at the growth interface and the obtained boundary layer thickness is similar to that estimated by analytical calculation. The effect of the crucible cover coating on the coupled O and C transport was investigated. The numerical results show that the C concentration in the grown silicon ingot can be reduced by about 60% if the pure graphite cover was replaced by a graphite cover with an inert material coating on it. However, the cover coating did not significantly affect the O concentration in the grown ingot. The numerical predictions of the C concentration showed satisfactory agreement with the experimental measurements.

© 2017 Elsevier Ltd. All rights reserved.

1. Introduction

Multi-crystalline silicon (mc-Si) ingot is the dominant material in the photovoltaic market at present and is expected to remain so in the foreseeable future. Directional solidification (DS) method is the leading technique for producing mc-Si ingots owing to its good feedstock tolerance, low production cost and easy operation. However, the DS process is accompanied by the transport of impurities, such as oxygen (O), carbon (C) [1], and their related reactants. O and C impurities in the grown ingots can significantly deteriorate the conversion efficiency of solar cells [2,3]. Effective control of O and C impurities in the silicon ingot is therefore essential to produce high quality solar cells. Numerous studies of the O and C transport in the DS process for mc-Si ingots have been carried out [4–13]. Many of these comprise local simulations [4–7] that just calculate the transport of impurities in the silicon melt. Some global simulations [8–13] take into account the gas transport of impurities. However, these simulations either neglected the C transport in the silicon melt [8–10] or didn't directly include the O and C segregation during the entire solidification process [11–13] so that the final distributions of O and C impurities in the silicon ingot cannot be predicted.

With the aid of the aforementioned numerical models, the effects of several process parameters and local furnace configurations on the impurity transport in the DS furnace have been investigated. Trempa et al. [14] studied the influence of growth rate on the C distribution in the silicon melt and crystal. Li et al. [8] analyzed the effects of argon flow rate and furnace pressure on the evaporation of SiO and concentration of CO at the melt surface in a DS furnace. Nakano et al. [15] pointed out that the heater positions could change the flow direction of the melt near the crucible wall and ultimately affects the O concentration in the melt. Bellmann et al. [16] designed a novel method for gas flow in a DS furnace and numerically evaluated its effect on impurity transport using a global impurity transport model [17]. Gao et al. [18,19] proposed a crucible cover (or a gas flow guidance device) to control the O and C transport in a small laboratory-scale DS furnace. Teng et al. [10,12] extended this idea to a large-size industrial DS furnace and numerically reported that the O and C concentrations in the silicon melt were affected by the position and geometry of the gas flow guidance device. Liu et al. [13] also numerically

* Corresponding author.
E-mail address: ljliu@mail.xjtu.edu.cn (L. Liu).

http://dx.doi.org/10.1016/j.ijheatmasstransfer.2017.01.092
0017-9310/© 2017 Elsevier Ltd. All rights reserved.

investigated the effect of crucible cover on the O and C transport in the large-size industrial DS furnace and reported that the C concentration in the silicon melt by using a graphite cover can be reduced by two orders of magnitude by using an inert material crucible cover or a graphite cover with an inert material coating on it. However, experimental results for the C concentration in the finally grown silicon ingot did not show the same benefits as those numerically reported [13] when the graphite crucible cover with coating was adopted in the DS furnace. For an accurate prediction of O and C concentrations in the grown ingot in the large-size industrial DS furnace, it is necessary to improve the global models of O and C transport as mentioned above.

In this study, transient global simulations of coupled O and C transport were implemented for the entire environment of an industrial DS furnace. Special attention was focused on modeling of the phase change as well as the O and C segregation during the silicon solidification process. Five chemical reactions were taken into account. The effect of crucible cover coating on the O and C concentrations in the grown ingot was investigated. The numerical results of C concentration in the ingot were compared with the experimental measurements obtained using Fourier transform infrared (FTIR) spectrometry.

2. Experimental setup

Fig. 1(a) shows the configuration of the industrial DS furnace. The DS system mainly consists of quartz crucible, susceptor, heat exchange block, graphite resistance heater, insulations and chamber wall. The silicon feed material is loaded into a quartz crucible with a volume of $84 \times 84 \times 42$ cm^3. The height of the silicon ingot is 24 cm. The crucible walls are supported by susceptors to avoid deformation at high temperature. The furnace is well sealed with a water-cooled wall and operates at a low pressure. Inert argon gas is used for purifying the growth environment. Thermocouple 1 (TC1) is installed near the top graphite resistance heater to monitor the temperature, which is used for controlling the heater power. The side insulation, labeled 8 in the figure, moves up in a prescribed way to first activate and then maintain the solidification process. Mc-Si ingots were grown in the same industrial DS furnace with a graphite cover with and without coating, respectively, using the same processing recipe and feedstock in the production line. The substitutional C in the grown ingots was measured by FTIR spectrometry.

3. Model description

3.1. Global model of heat transfer

A transient global model of heat transfer, taking into account the melt convection, argon flow, solid thermal conduction, thermal radiation, and phase change, was developed for the DS furnace. The entire furnace was equivalently simplified to be axisymmetric and divided into a number of sub-domains, as shown in the right part of Fig. 1(a). To compromise the computational convenience and accuracy, the major assumptions in the global model are as follows: (1) all radiative surfaces are assumed to be diffuse-gray; (2) the silicon melt flow is laminar and incompressible; (3) the Boussinesq assumption is applied to the melt flow; (4) the low Mach approximation and the ideal gas law are applied to the argon gas. The Reynolds number of the argon gas flow in this industrial DS furnace is of the order of 4320 and the standard $k-\varepsilon$ turbulence model [20] was used. It is worth noting that the DS furnace under consideration in this study is in three dimension (3D). However, the silicon melt structure presents some symmetric characteristics in the square shaped crucible except at the corner region

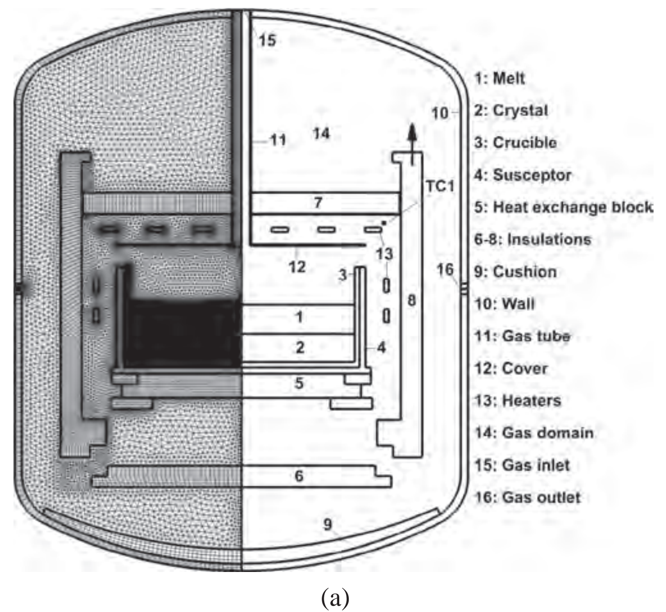

(a)

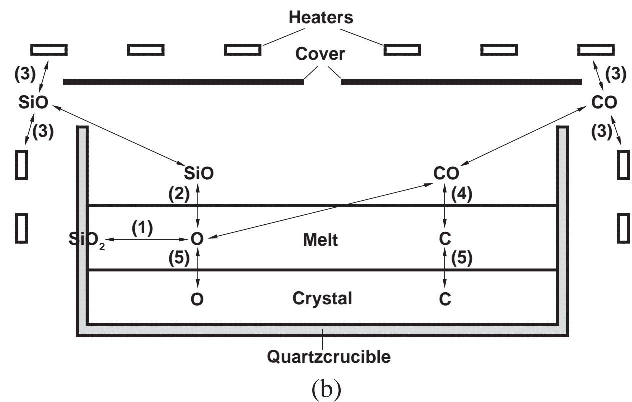

(b)

Fig. 1. Configuration/computation grids of the industrial DS furnace (a) and pathway of the coupled O/C transport in the furnace chamber (b).

[21]. Besides, the thermal field in the silicon domain, the melt-crystal interface shape and the silicon melt flow are dominated by the radial interaction between the silicon and the quartz crucible rather than its asymmetry in the circumferential direction because of the huge difference in the thermal properties of the silicon material and quartz crucible. Therefore, to release computational load, the 3D systems were equivalently simplified to two dimensional (2D) axisymmetric under the condition that the thermal resistance remained unchanged in the DS furnace. This simplification is widely used to study the characteristics of heat and mass transfer in the industrial DS furnaces [12,22–24].

To track the melt-crystal (m-c) interface evolution during the entire solidification process, an enthalpy formulation technique based on a fixed-grid methodology [25] was used to model the phase change problem in the silicon region during the growth process. The governing equations for the silicon domain are expressed in the following forms:

$$\nabla \cdot \vec{u} = 0, \tag{1}$$

$$\rho \frac{\partial \vec{u}}{\partial t} + \rho \vec{u} \cdot \nabla \vec{u} = -\nabla p + \nabla \cdot [\mu(\nabla \vec{u} + \nabla \vec{u}^T)] - \beta \rho \vec{g}(h - h_{ref})/C_p + \vec{S}_u, \tag{2}$$

$$\rho\frac{\partial h}{\partial t}+\rho\vec{u}\cdot\nabla h=\nabla\cdot\left(\frac{\lambda}{C_p}\nabla h\right)+S_h, \quad (3)$$

where $\vec{u}$ is the velocity, ρ is the density, p is the pressure, μ is the dynamic viscosity, $\vec{g}$ is the gravity acceleration vector, β is the thermal expansion coefficient, h is the sensible enthalpy, h_{ref} is the reference sensible enthalpy, λ is the heat conductivity, and C_p is the heat capacity. The source term $\vec{S}_u$ in Eq. (2) is introduced to drop the velocity to zero when the silicon melt has fully solidified in a grid cell during the phase change. The source term S_h in Eq. (3) represents the rate of volumetric latent heat change during the silicon solidification process. A concept of liquid fraction g_l in each cell volume is introduced in the fixed-grid technique. Detailed information can be found in Ref. [25]. This enthalpy formulation based on the fixed-grid technique has been successfully used to model crystal growth [7,26,27].

Along the melt-gas surface, both the gas shear stress and Marangoni tension were considered. Zero radial gradients for all the variables are applied along the centerline of the furnace. Temperature continuity and heat flux conservation are kept at all interior boundaries between any two neighboring sub-domains. In the current simulation, the argon flow rate is 20 L/min and the furnace pressure is 0.6 bar. The temperature of the outer wall of the chamber is set to 300 K. Temperature of TC1 and movement of the side insulation correspond to the values in the actual run.

3.2. Coupled model of oxygen and carbon transport

Based on the global thermal and flow fields, the coupled O and C transport was simulated. A generally accepted pathway for the O and C transport in a DS furnace is as follows [8,11], which is also shown in Fig. 1(b): (1) Dissolution of the quartz crucible releases O atoms into the silicon melt; (2) The dissolved O atoms in the silicon melt are transported to the melt surface by diffusion and convection and evaporate into the argon gas in the form of vapor phase SiO; (3) The SiO is then carried away by the argon flow to heater surfaces and reacts with carbon to form CO; (4) The reactant CO is transported back to the melt surface by convection and diffusion and then dissolves into the silicon melt in the form of C and O atoms; (5) Finally, the C and O atoms at the m-c interface segregate into the growing crystal.

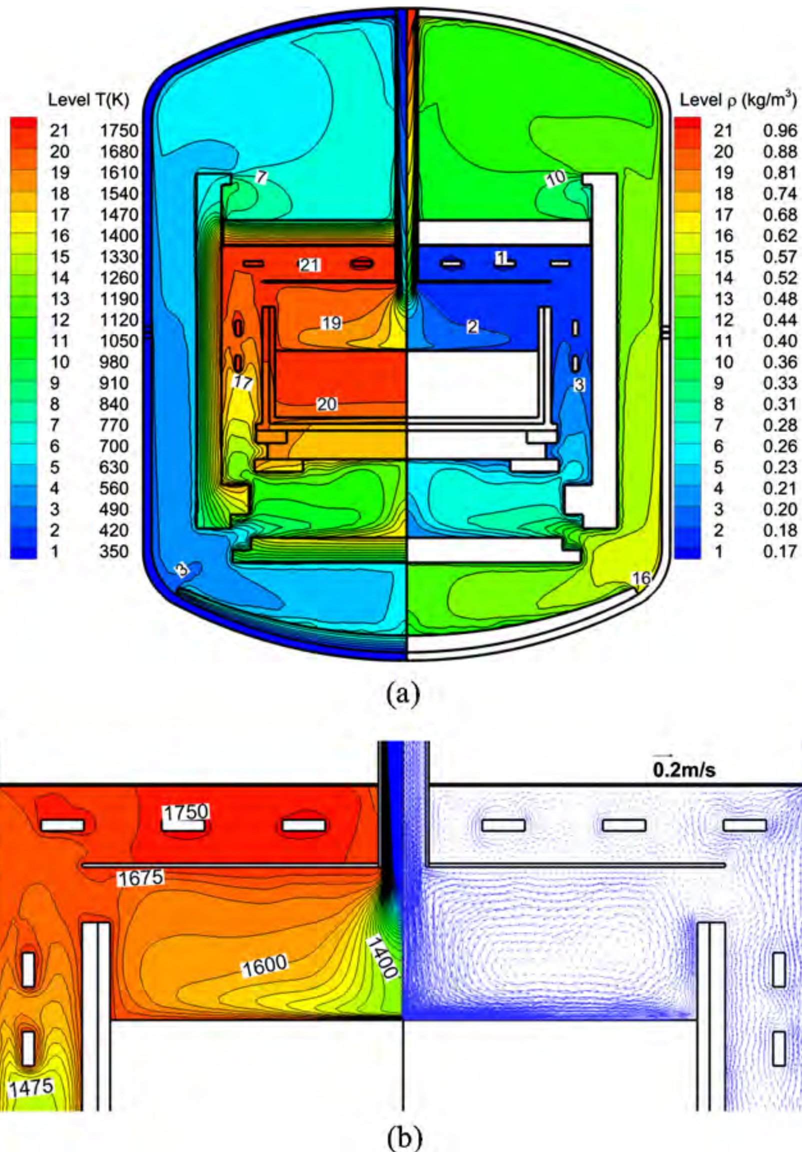

Fig. 2. Global temperature and density distributions (a) and local temperature and velocity above the melt surface (b) in the DS furnace (t = 4 h).

The chemical equations corresponding to the above five reactions are given below. On the inside wall of the quartz crucible:

$$SiO_2(s) \leftrightarrow Si(m) + 2O(m). \tag{4}$$

At the melt-gas interface (for O):

$$Si(m) + O(m) \leftrightarrow SiO(g). \tag{5}$$

At the graphite fixtures surfaces:

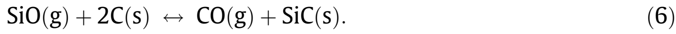

$$SiO(g) + 2C(s) \leftrightarrow CO(g) + SiC(s). \tag{6}$$

At the melt-gas interface (for C):

$$CO(g) \leftrightarrow C(m) + O(m). \tag{7}$$

At the melt-crystal interface:

$$O(m) \leftrightarrow O(c), \tag{8a}$$

$$C(m) \leftrightarrow C(c). \tag{8b}$$

In the above equations, the index symbols (s), (m), (g) and (c) denote solid, melt, gas and crystal, respectively.

In the enthalpy formulation technique, which is based on a fixed-grid methodology for the phase change that occurs during the silicon solidification process, the silicon region (melt and crystal) is treated as a unitary calculation domain and the m-c interface is not solved explicitly. Therefore, instead of separately solving the governing equations for O and C transport in the silicon melt and crystal, as is done in Refs. [8,11], the governing equations for O transport in the silicon region are written as follows:

$$\begin{aligned}&\frac{\partial}{\partial t}(\rho\omega_O) + \nabla\cdot(\rho g_l \vec{u}\,\omega_{O,m}) = -\nabla\cdot(-\rho g_l D_{O,m}\omega_{O,m} - (1-g_l)\rho D_{O,c}\omega_{O,c})\\ &\omega_O = g_l\omega_{O,m} + (1-g_l)\omega_{O,c}\\ &\omega_{O,c} = k_{Oseg}\omega_{O,m}\end{aligned} \tag{9}$$

where ω_O is the mass fraction of O atoms, $D_{O,m}$ and $D_{O,c}$ are the molecular diffusivity for O atoms in the silicon melt and crystal, respectively, and k_{Oseg} is the segregation coefficient of O in silicon. The index symbols O denotes the oxygen impurity. The governing equation for C transport in the silicon region has the same expression form as that for O. In the current simulation, the molecular diffusivities for both O and C in the melt and crystal are taken to be 5.0×10^{-8} m^2/s [28] and 5.0×10^{-11} m^2/s [8], respectively. The segregation coefficients of O and C in silicon are 1.25 [29] and 0.07 [30], respectively.

The governing equations for the transport of the SiO and CO species in the argon gas are as follows:

$$\frac{\partial}{\partial t}(\rho\omega_{SiO}) + \nabla\cdot(\rho\omega_{SiO}\vec{u}_{Ar}) = -\nabla\cdot\left[\left(\rho D_{SiO} + \frac{\mu_t}{Sc_t}\right)\nabla\omega_{SiO}\right], \tag{10}$$

$$\frac{\partial}{\partial t}(\rho\omega_{CO}) + \nabla\cdot(\rho\omega_{CO}\vec{u}_{Ar}) = -\nabla\cdot\left[\left(\rho D_{CO} + \frac{\mu_t}{Sc_t}\right)\nabla\omega_{CO}\right], \tag{11}$$

where ω_{SiO} and ω_{CO} are the mass fractions of SiO and CO in the argon gas region, respectively, μ_t is the turbulent viscosity, and $\vec{u}_{Ar}$ is the argon gas flow velocity. The turbulent Schmidt number Sc_t is equal to 0.7. D_{SiO} and D_{CO} are the molecular diffusivities of SiO and CO in the argon gas, respectively, which can be expressed as [31]:

$$D_{SiO} = 8.62611 \times 10^{-6}\frac{T^{1.75}}{p}, \tag{12}$$

$$D_{CO} = 1.79548 \times 10^{-5}\frac{T^{1.75}}{p}. \tag{13}$$

The boundary conditions for the impurity species transport in the silicon and argon gas regions are as follows:

(a) On the inside wall of the quartz crucible, considering the chemical reactions between the Si_3N_4 coating layer and the quartz crucible and between the Si_3N_4 coating layer and silicon melt, the equilibrium concentration of O atoms can be expressed as [32]:

$$\begin{aligned}&c_O = 0.5 \times 10^{23} \times \frac{a}{1-a}\ \text{atom/cm}^3,\\ &a = 1.32 \times \exp\left(\frac{-7150}{T} - 6.99\right)\end{aligned} \tag{14}$$

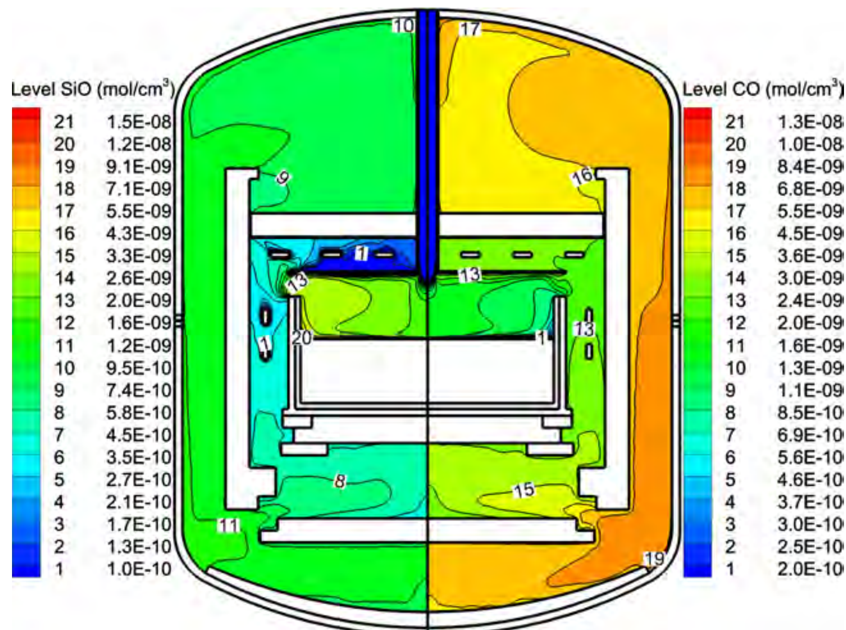

Fig. 3. SiO and CO distributions in the DS furnace (t = 4 h).

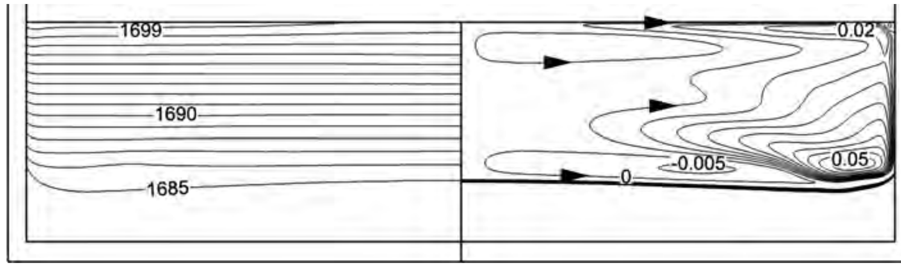

Fig. 4. Temperature, stream function and m-c interface shape in the growing silicon (t = 4 h). Intervals for temperature and stream function are $\Delta T = 1$ K and $\Delta\psi = 0.005$ kg/s, respectively.

For the C atoms at the inside wall of the crucible, zero flux boundary condition is applied.

(b) At the melt-gas interface, O, C, SiO and CO coexist. Equilibrium relationships for the same element between the silicon melt and argon gas are given as follows [31]:

$$c_{SiO} = \frac{101325}{R_g T}\frac{c_O}{c_{Si}}e^{-21000/T+17.8}, \quad (15)$$

$$c_{CO} = \frac{101325}{R_g T}\frac{c_O}{c_{Si}}\frac{c_C}{c_{Si}}e^{-5210/T+14.6}, \quad (16)$$

where c_{SiO} and c_{CO} are the molar concentrations of SiO and CO in the argon gas, respectively, c_O and c_C are the molar concentrations of O and C in the silicon melt, respectively, and R_g is the universal gas constant, which is equal to 8.314 J/mol·K.

Two more boundary conditions are needed to solve the four unknown variables at the melt-gas surface according to the law of mass conservation:

$$c_{Ar}\left(D_{SiO} + \frac{\mu_t}{\rho_{Ar}Sc_t}\right)\nabla\left(\frac{c_{SiO}}{c_{Ar}}\right) + c_{Ar}\left(D_{CO} + \frac{\mu_t}{\rho_{Ar}Sc_t}\right)\nabla\left(\frac{c_{CO}}{c_{Ar}}\right) = c_{Si}D_O\nabla\left(\frac{c_O}{c_{Si}}\right), \quad (17)$$

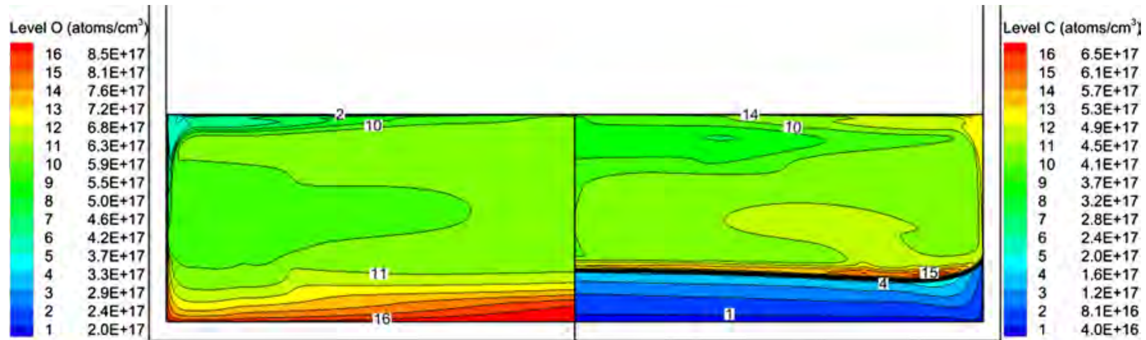

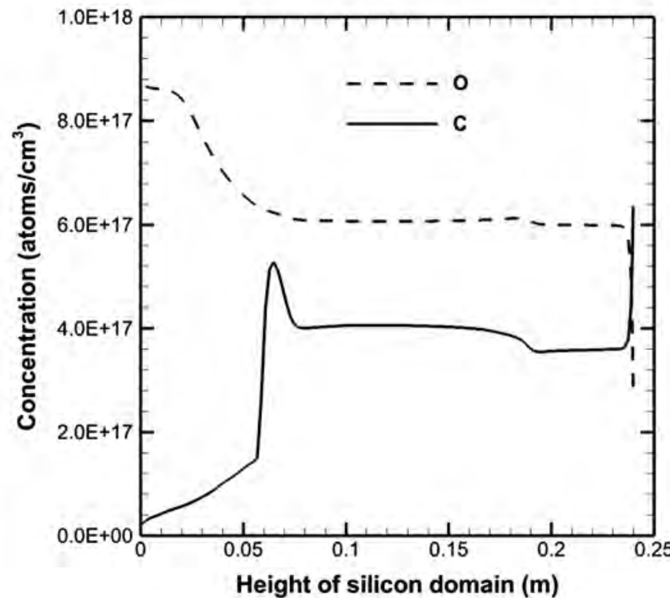

Fig. 5. Oxygen and Carbon distributions in the growing silicon (a) and along the centerline of the growing silicon (b) (t = 4 h).

$$c_{Ar}\left(D_{CO}+\frac{\mu_t}{\rho_{Ar}Sc_t}\right)\nabla\left(\frac{c_{CO}}{c_{Ar}}\right)=c_{Si}D_C\nabla\left(\frac{c_C}{c_{Si}}\right). \tag{18}$$

(c) The SiO reacts with carbon at the surfaces of the hot graphite fixtures to generate CO. The reaction is assumed to be reversible and the Gibbs free energy of the reaction is expressed as follows [31]:

$$\begin{aligned}&\Delta G=-81300+3.02T\ \text{J/mol},\quad T<1640\ \text{K},\\&\Delta G=-22100-33.1T\ \text{J/mol},\quad 1640\ \text{K}<T<1687\ \text{K},\\&\Delta G=-72100-3.44T\ \text{J/mol},\quad T>1687\ \text{K}\end{aligned} \tag{19}$$

The equilibrium constant of the reaction is $K=e^{-\Delta G/RT}$. The coupled boundary conditions at the graphite fixtures' surfaces can be expressed as:

$$c_{Ar}\left(D_{SiO}+\frac{\mu_t}{\rho_{Ar}Sc_t}\right)\nabla\left(\frac{c_{SiO}}{c_{Ar}}\right)=-c_{Ar}\left(D_{CO}+\frac{\mu_t}{\rho_{Ar}Sc_t}\right)\nabla\left(\frac{c_{CO}}{c_{Ar}}\right), \tag{20}$$

$$\frac{c_{CO}}{c_{SiO}}=K. \tag{21}$$

(d) At the argon gas inlet, the concentrations of SiO and CO are set to zero. At other solid component surfaces, zero fluxes of SiO and CO are applied. At the argon gas outlet, zero gradients of SiO and CO are used. Zero radial gradients for all the species are applied along the centerline of the fluid regions in the furnace.

The relationship between the mass fraction ω and the molar concentration c in the aforementioned equations and boundary conditions is $c=\rho\omega/M$, where M is the atomic weight of the impurity species. The measured concentrations of O and C in the silicon feedstock are used as the initial concentrations for the simulations, which are about 1.39×10^{17} atoms/cm^3 (2.5 ppma) and 0.693×10^{17} atoms/cm^3 (1.25 ppma) for O and C, respectively, distributed uniformly in the silicon melt. The governing equations and the boundary conditions for the flow, temperature and impurity transport are discretized and solved by the finite volume method. A structured/unstructured combined mesh scheme [33] was applied to improve the computation efficiency as shown in Fig. 1(a). In this study, a total of 88,600 cell volumes was used for the entire furnace. The silicon domain was meshed with a cell size of 1.5×1.5 mm with refinement at the boundaries. A new finer grid with a cell size of 0.75×0.75 mm for the silicon domain, resulting in a total of 268,300 cell volumes for the entire furnace, were used to test the grid independence. The comparison of the O and C concentration profiles along the centerline of the silicon crystal leads to a mean relative deviation of 3.89% and 4.38%, respectively, between the two cases. Considering the huge increase in the computational cost for the new grid, the current cell size of 1.5×1.5 mm for the silicon domain is numerically acceptable. The time step is taken to be 10 s.

4. Results and discussions

4.1. Simulations for a graphite crucible cover without coating

Fig. 2(a) shows the global temperature field and the density distribution of argon gas 4 h after the start of the solidification process (t = 4 h). The furnace chamber was divided into two thermal zones

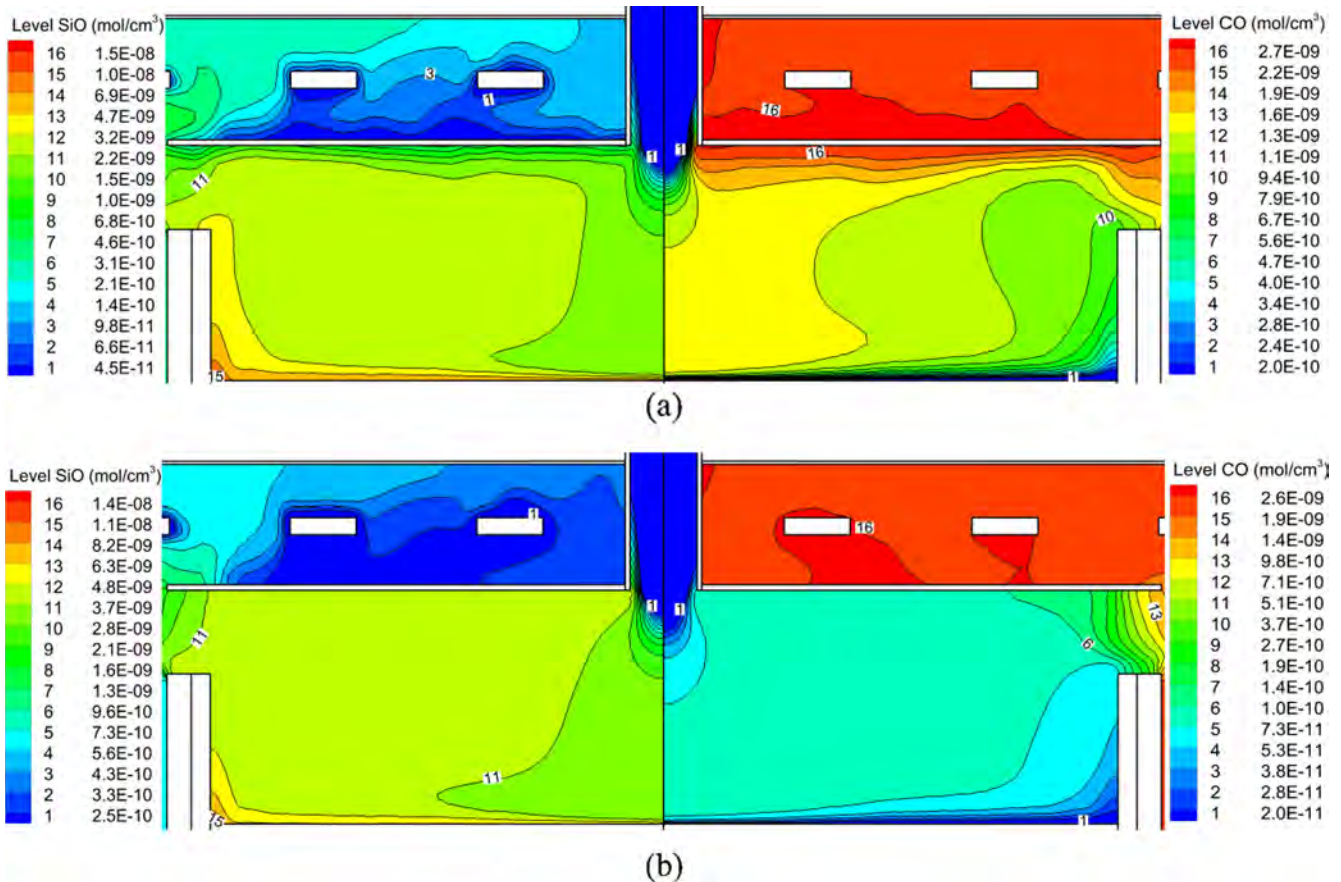

Fig. 6. Local SiO and CO distributions in the argon gas under the graphite cover without (a) and with (b) coating (t = 4 h).

by the insulation cage: the hot zone inside the cage and the cold zone outside the cage. The temperature varies from 300 K at the chamber outer wall to 1750 K in the top heater. The solidification process was maintained by extracting radiation heat loss from the gap between the side and bottom insulation layers. Fig. 2(b) gives the local temperature and velocity fields of the argon gas above the melt surface. A strong gas flow circulation is formed above the melt surface due to the injecting of cool argon gas through the centrally positioned gas inlet, leading to a large temperature variation in this region. Owing to the large temperature variation, the density of argon gas changes significantly in the region above the central melt surface. The SiO and CO concentrations in the argon gas are shown in Fig. 3. The calculated mass fractions of SiO and CO are converted into molar concentrations. For the graphite cover without coating, the chemical reaction was considered on the cover surface. It can be seen that the basic order of SiO concentration is 10^{-9} mol/cm^3. The maximum concentration is 1.5×10^{-8} mol/cm^3, which appears at the corner region surrounded by the crucible and the silicon melt. SiO evaporates from the melt surface and is carried away by the argon flow to the entire furnace chamber. At the heater and cover surfaces, SiO reacts with carbon to produce CO, leading to a relatively low SiO concentration at these surfaces. The reactant CO originating from the cover is then directly transported back to the melt surface by the strong argon gas circulation. The basic order of CO concentration in the furnace chamber is 10^{-9} mol/cm^3.

Fig. 4 shows the temperature and stream function of the silicon melt and the m-c interface (bold black line on the right) 4 h after the start of the solidification process. We can observe three vortices in the melt which are driven by buoyancy force. The largest, on the right, dominates the melt flow and flows downward along the crucible inside wall. Under the effect of the argon gas shear stress, the silicon melt flows outwards along the melt surface, resulting in a clockwise vortex at the upper layer. It is also found that the m-c interface is slightly convex to the silicon melt at the central region and concave at the periphery near the crucible wall.

Fig. 5(a) shows the O and C concentrations in the silicon melt and crystal. The concentration of oxygen is large at the silica crucible wall where the O atoms dissolve into the melt. The dissolved O atoms are transported into the silicon melt, part of which segregate into the growing crystal at the growth interface. The rest are carried to the melt surface and evaporate as SiO phase into the argon gas flow, leading to a small O concentration near the melt surface. Due to the small segregation coefficient $k_{Cseg} = 0.07$, most C atoms are pushed into the silicon melt, causing a relatively high C concentration and C concentration gradient at the m-c interface in the melt. A region with relatively high C concentration and low O concentration exists at the top layer of the melt due to the strong gas flow circulation above the melt surface, which carries the SiO evaporated from the melt surface and consumes them to produce CO at the surface of the graphite cover, then brings CO back to the melt surface, as shown in Figs. 2(b) and 3. The O and C concentration profiles along the centerline of the growing silicon in Fig. 5 (a) are presented in Fig. 5(b). The numerical results show that the boundary layer thickness of C impurity at the growth interface is about 13.0 mm. The boundary layer thickness δ_D of solute segregation at the growth interface in the Bridgman crystal growth has been estimated by [34]:

$$\delta_D = 5\sqrt{\frac{\nu \times H}{V_\infty}}\left(\frac{D}{\nu}\right)^n, \quad (22)$$

where ν, H, V_∞ and D are the kinematic viscosity, height of the melt, melt velocity and diffusion coefficient, respectively. The exponent n is in the range $1/2 \geqslant n \geqslant 1/3$ [34]. Using the values of $\nu = 2.7 \times 10^{-7}$ m^2/s [28], $H = 0.17$ m, $V_\infty = 0.0015$ m/s and $D = 5.0 \times 10^{-8}$ m^2/s [28], the boundary layer thickness at the growth interface are estimated to be 11.9–15.8 mm, which is similar to our numerical simulation result. The impurity segregation at the growth interface can be successfully caught by the enthalpy formulation based on the fixed-grid technique used in this study.

4.2. Effect of the crucible cover coating on the coupled O/C transport

Experiments were performed in the same industrial DS furnace under the graphite cover without and with coating, respectively, using the same processing recipe. The cover coating was made of inert materials. When using the graphite cover without coating, the evaporated SiO reacts with the cover to produce CO. When using the one with coating, such a chemical reaction does not occur on the cover surface. Therefore, in the numerical simulations, the chemical reaction on the cover surface was considered for the graphite cover without coating, while it was not taken into account for the cover with coating and zero fluxes of SiO and CO were applied on the cover surface. Fig. 6(a) and (b) shows the local SiO and CO

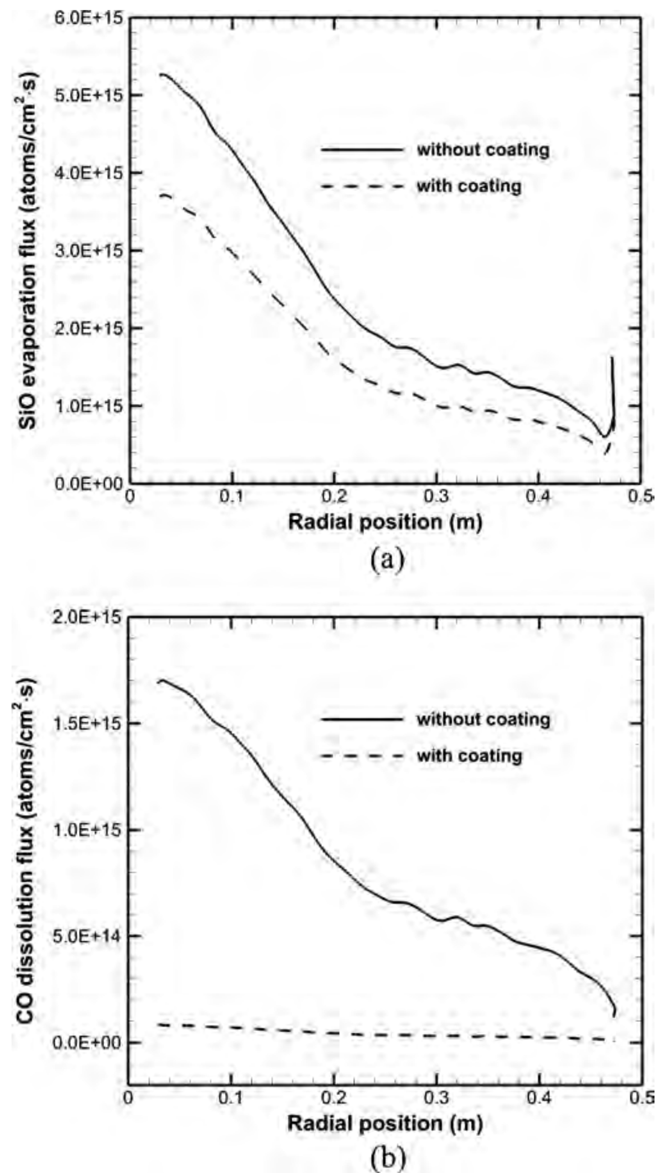

Fig. 7. SiO evaporation flux (a) and CO dissolution flux (b) along the melt surface (t = 4 h).

distributions above the melt surface for the cases without and with coating, respectively. In the case without coating, as shown in Fig. 6(a), SiO evaporates from the melt surface and reacts with carbon at the heater and crucible cover's surfaces to produce CO gas. CO originating from the cover is then directly transported back to the melt surface by the strong gas circulation in the furnace. While for the case with coating, as shown in Fig. 6(b), the graphite heater becomes the unique CO source. CO can only be transported back to the melt surface through the gap between the crucible top edge and the cover by diffusion, resulting in a large concentration gradient at the gap. This is the reason that the CO concentration above the melt surface in Fig. 6(a) is larger than that in Fig. 6(b). Fig. 7(a) and (b) shows the SiO evaporation flux and CO dissolution flux along the melt surface, respectively. We find that the SiO evaporation flux along the melt surface for the graphite crucible without coating is larger than that with coating, owing to the fact that SiO is consumed by the chemical reaction on the cover surface, leading to less SiO transported back to the melt surface. While the CO dissolution flux along the melt surface for the cover without coating is significantly higher than that with coating. That means that more C atoms are dissolved into the silicon melt, transported to the m-c interface, and then segregate into the silicon crystal for the graphite cover without coating.

The O and C concentrations in the grown ingots at the end of the solidification process are shown in Fig. 8. We find that the O concentration shows no significant difference between both cases. This is surprising because the higher SiO evaporation flux along the melt surface should lead a lower O concentration for the graphite cover without coating. The reason for this result is that the CO dissolution flux along the melt surface for the cover without coating is significantly higher than that with coating, leading to no significant difference of O net flux (SiO evaporation flux subtracted by CO dissolution flux) between the two cases, as shown in Fig. 9. In the finally grown ingots, the C concentration increases gradually from bottom to top. Unlike the O concentration, the cover coating strongly affect the C concentration in the grown silicon ingots.

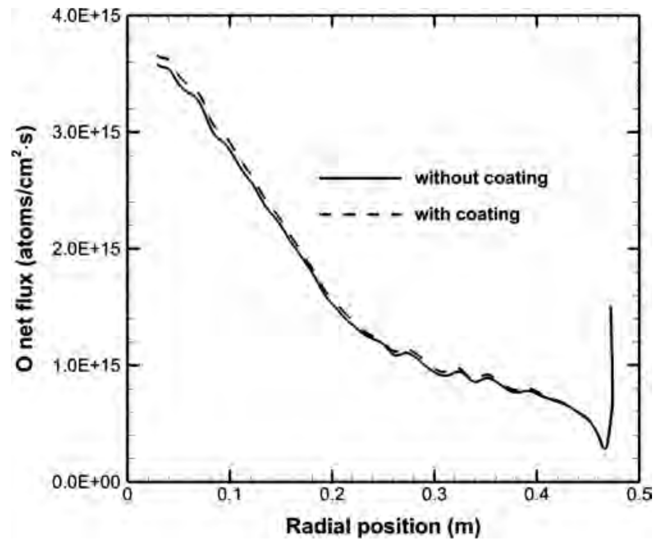

Fig. 9. Oxygen net flux along the melt surface (t = 4 h).

Fig. 10 shows the carbon concentration along the centerline of the grown ingots. It can be seen that the C concentration is reduced by 60% if the graphite cover with coating is used. The calculated

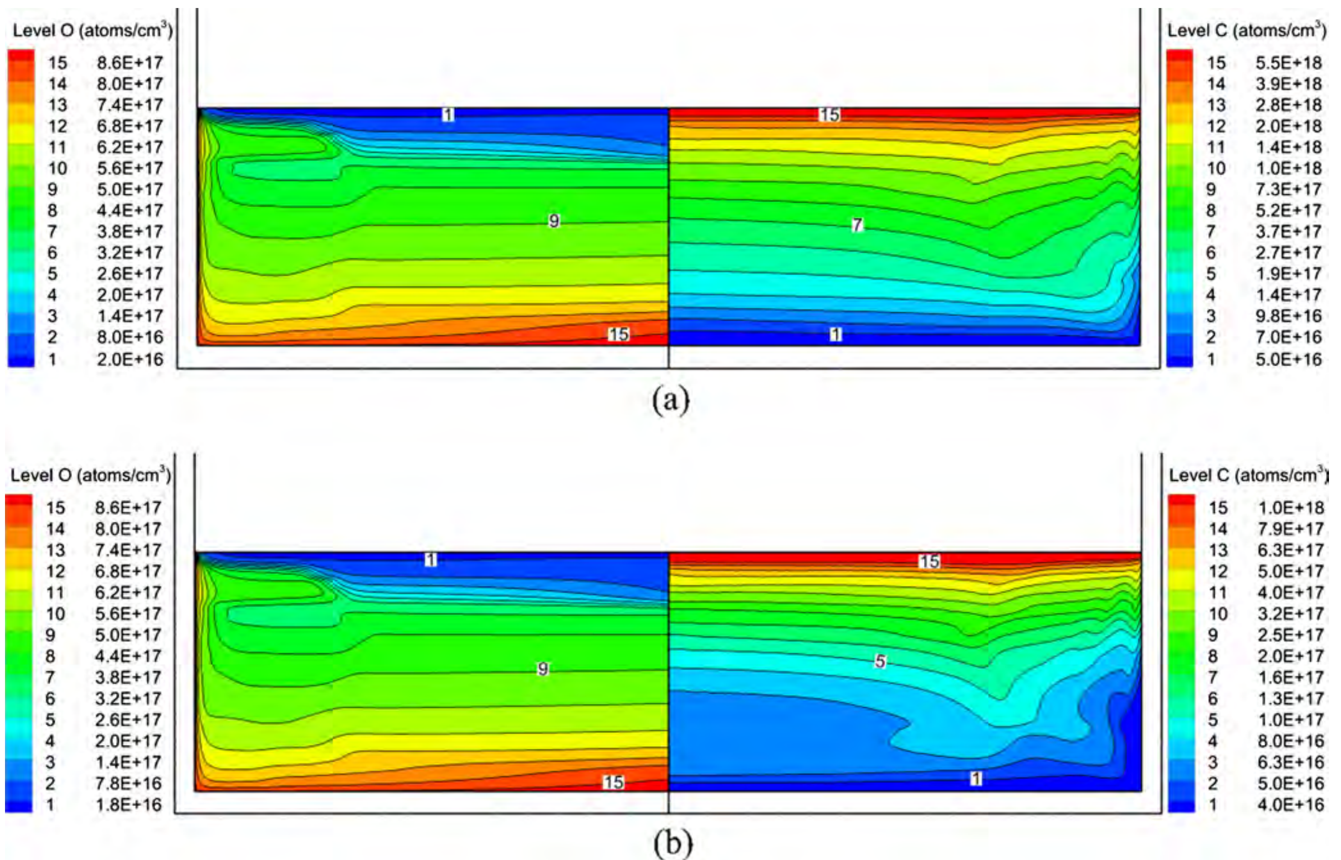

Fig. 8. Oxygen (left part) and Carbon (right part) distributions in the crystal at the end of the solidification process under the graphite cover without (a) and with (b) coating.

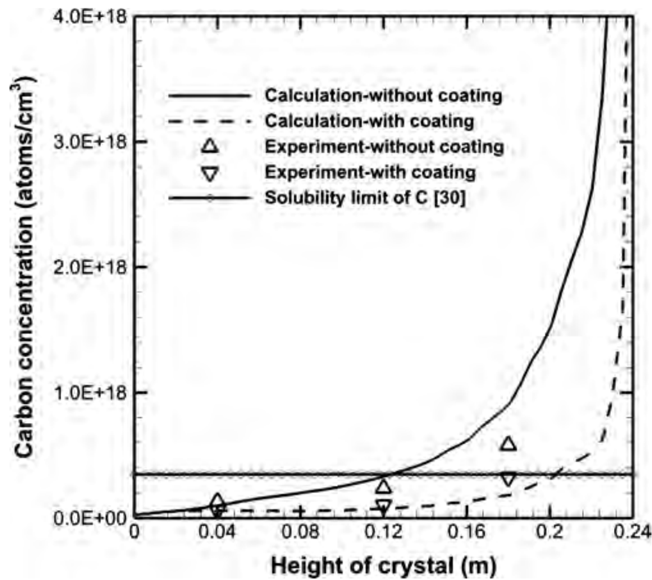

Fig. 10. Carbon concentration along the centerline of the grown ingot.

results reveal that the maximum C solubility limit of 3.5×10^{17} atoms/cm^3 [30] in the silicon crystal is exceeded at a fraction of the grown ingot equal to 0.521 for the cover without coating, while this fraction is equal to 0.846 with coating, which indicates that less silicon carbide (SiC) precipitates formed in the ingot produced using the cover with coating. The calculated results show good agreement with the measurements at the bottom and middle regions of the ingots. However, for the graphite cover without coating, the measured values are smaller than the calculated values in the top region. This is because that only the substitutional C can be measured by FTIR spectrometry, while other states of C, such as SiC precipitates, are undetected. The experimental and calculated results of the C concentration in the grown silicon ingots do not show the same benefits as reported in Ref. [13] when an inert material cover or a graphite cover with coating was used. This may be attributed to the fact that the impurity segregation phenomenon was not simulated and consequently the C impurity in the silicon feedstock was not considered in the simulations in Ref. [13].

5. Conclusions

A transient global model of coupled O and C transport based on a fully coupled calculation of the thermal and flow fields was implemented for a large-size industrial DS furnace. Special attention was focused on the modeling of the phase change as well as on the O and C segregations during the silicon solidification process. The effects of crucible cover coating on the O and C concentrations in the grown silicon ingots were investigated. We found that the C concentration can be reduced by about 60% if the graphite cover without coating was replaced by a cover with coating. The cover coating, however, did not significantly influence the O concentration in the grown ingot. The numerical predictions show good agreement with the experimental measurements.

Acknowledgements

This work was supported by the National Natural Science Foundation of China (Nos. 51676154 and 51406156) and Natural Science Basic Research Plan in Shaanxi Province of China (No. 2014JZ014).

References

[1] H. Matsuo, R.B. Ganesh, S. Nakano, L.J. Liu, K. Arafune, Y. Ohshita, M. Yamaguchi, K. Kakimoto, Analysis of oxygen incorporation in unidirectionally solidified multicrystalline silicon for solar cells, J. Cryst. Growth 310 (2008) 2204–2208.
[2] T. Saitoh, X. Wang, H. Hashigami, T. Abe, T. Igarashi, S. Glunz, S. Rein, W. Wettling, I. Yamasaki, H. Sawai, H. Ohtuka, T. Warabisako, Suppression of light degradation of carrier lifetimes in low-resistivity CZ-Si solar cells, Sol. Energy Mater. Sol. Cells 65 (2001) 277–285.
[3] O. Breitenstein, J.P. Rakotoniaina, M.H. Al Rifai, M. Werner, Shunt types in crystalline silicon solar cells, Prog. Photovolt. Res. Appl. 12 (2004) 529–538.
[4] L.J. Liu, S. Nakano, K. Kakimoto, Carbon concentration and particle precipitation during directional solidification of multicrystalline silicon for solar cells, J. Cryst. Growth 310 (2008) 2192–2197.
[5] C. Reimann, M. Trempa, T. Jung, J. Friedrich, G. Müller, Modeling of incorporation of O, N, C and formation of related precipitates during directional solidification of silicon under consideration of variable processing parameters, J. Cryst. Growth 312 (2010) 878–885.
[6] Y.Y. Teng, J.C. Chen, C.W. Lu, C.Y. Chen, The carbon distribution in multicrystalline silicon ingots grown using the directional solidification process, J. Cryst. Growth 312 (2010) 1282–1290.
[7] M.P. Bellmann, E.A. Meese, L. Arnberg, Impurity segregation in directional solidified multi-crystalline silicon, J. Cryst. Growth 312 (2010) 3091–3095.
[8] Z.Y. Li, L.J. Liu, W.C. Ma, K. Kakimoto, Effects of argon flow on impurities transport in a directional solidification furnace for silicon solar cells, J. Cryst. Growth 318 (2011) 304–312.
[9] Y.Y. Teng, J.C. Chen, C.W. Lu, H.I. Chen, C. Hsu, C.Y. Chen, Effects of the furnace pressure on oxygen and silicon oxide distribution during the growth of multicrystalline silicon ingots by the directional solidification process, J. Cryst. Growth 318 (2011) 224–229.
[10] Y.Y. Teng, J.C. Chen, C.W. Lu, C.Y. Chen, Numerical investigation of oxygen impurity distribution during multicrystalline silicon crystal growth using a gas flow guidance device, J. Cryst. Growth 360 (2012) 12–17.
[11] B. Gao, S. Nakano, K. Kakimoto, Global simulation of coupled carbon and oxygen transport in a unidirectional solidification furnace for solar cells, J. Electrochem. Soc. 157 (2010) H153–H159.
[12] Y.Y. Teng, J.C. Chen, B.S. Huang, C.H. Chang, Numerical simulation of impurity transport under the effect of a gas flow guidance device during the growth of multicrystalline silicon ingots by the directional solidification process, J. Cryst. Growth 385 (2014) 1–8.
[13] L.J. Liu, X.F. Qi, W.C. Ma, Z.Y. Li, Y.F. Zhang, Control of the gas flow in an industrial directional solidification furnace for production of high purity multicrystalline silicon ingots, Int. J. Photoenergy 215 (2015) 10 Article ID 513639.
[14] M. Trempa, C. Reimann, J. Friedrich, G. Müller, The influence of growth rate on the formation and avoidance of C and N related precipitates during directional solidification of multicrystalline silicon, J. Cryst. Growth 312 (2010) 1517–1524.
[15] S. Nakano, B. Gao, K. Kakimoto, Relationship between oxygen impurity distribution in multicrystalline solar cell silicon and the use of top and side heaters during manufacture, J. Cryst. Growth 375 (2013) 62–66.
[16] M.P. Bellmann, B. Panjwani, M. Syvertsen, E.A. Meese, Dynamic simulation of impurity transport and chemical reactions in a Bridgman furnace for directional solidification of multi-crystalline silicon, J. Cryst. Growth 369 (2013) 47–54.
[17] M.P. Bellmann, D. Lindholm, M. M'Hamdi, A novel method for gas flow and impurity control in directional solidification of multi-crystalline silicon, J. Cryst. Growth 399 (2014) 33–38.
[18] B. Gao, X.J. Chen, S. Nakano, K. Kakimoto, Crystal growth of high-purity multicrystalline silicon using a unidirectional solidification furnace for solar cells, J. Cryst. Growth 312 (2010) 1572–1576.
[19] B. Gao, S. Nakano, K. Kakimoto, Effect of crucible cover material on impurities of multicrystalline silicon in a unidirectional solidification furnace, J. Cryst. Growth 318 (2011) 255–258.
[20] B.E. Launder, D.B. Spalding, The numerical computation of turbulent flows, Comput. Methods Appl. Mech. Eng. 3 (1974) 268–289.
[21] A. Popescu, D. Vizman, Numerical study of melt convection and interface shape in a pilot furnace for unidirectional solidification of multicrystalline silicon, Cryst. Growth Des. 12 (2012) 320–325.
[22] J.A. Wei, H. Zhang, L.L. Zheng, C.L. Wang, B. Zhao, Modeling and improvement of silicon ingot directional solidification for industrial production systems, Sol. Energy Mater. Sol. Cells 93 (2009) 1531–1539.
[23] S. Wang, H.S. Fang, C.J. Zhao, Z. Zhang, M.J. Zhang, J.F. Xu, Gas flow optimization during the cooling of multicrystalline silicon ingot, Int. J. Heat Mass Transfer 84 (2015) 370–375.
[24] L.J. Liu, Q.H. Yu, X.F. Qi, W.H. Zhao, G.X. Zhong, Controlling solidification front shape and thermal stress in growing quasi-single-crystal silicon ingots: process design for seeded directional solidification, Appl. Therm. Eng. 91 (2015) 225–233.
[25] V.R. Voller, C. Prakash, A fixed grid numerical modeling methodology for convection-diffusion mushy region phase-change problems, Int. J. Heat Mass Transfer 30 (1987) 1709–1719.
[26] W.C. Ma, L.L. Zhao, G.Q. Ding, Y. Yang, T.Z. Lv, M. Wu, L.J. Liu, Numerical study of heat transfer during sapphire crystal growth by heat exchanger method, Int. J. Heat Mass Transfer 72 (2014) 452–460.

[27] B. Gao, S. Nakano, H. Harada, Y. Miyamura, T. Sekiguchi, K. Kakimoto, Reduction of polycrystalline grains region near the crucible wall during seeded growth of monocrystalline silicon in a unidirectional solidification furnace, J. Cryst. Growth 352 (2012) 47–52.
[28] L.J. Liu, S. Nakano, K. Kakimoto, Investigation of oxygen distribution electromagnetic CZ-Si melts with a transverse magnetic field using 3D global modeling, J. Cryst. Growth 299 (2007) 48–58.
[29] Y. Yatsurugi, N. Akiyama, Y. Endo, T. Nozaki, Concentration, solubility, and equilibrium distribution coefficient of nitrogen and oxygen in semiconductor silicon, J. Electrochem. Soc. 120 (1973) 975–979.
[30] T. Nozaki, Y. Yatsurugi, N. Akiyama, Concentration and behavior of carbon in semiconductor silicon, J. Electrochem. Soc. 117 (1970) 1566–1568.
[31] D.E. Bornside, R.A. Brown, T. Fujiwara, H. Fujiwara, T. Kubo, The effects of Gas-phase convection on carbon contamination of Czochralski-grown silicon, J. Electrochem. Soc. 142 (1995) 2790–2804.
[32] H. Matsuo, R.B. Ganesh, S. Nakano, L.J. Liu, Y. Kangawa, K. Arafune, Y. Ohshita, M. Yamaguchi, K. Kakimoto, Thermodynamical analysis of oxygen incorporation from a quartz crucible during solidification of multicrystalline silicon for solar cell, J. Cryst. Growth 310 (2008) 4666–4671.
[33] Z.Y. Li, L.J. Liu, W.C. Ma, K. Kakimoto, Effects of argon flow on heat transfer in a directional solidification process for silicon solar cells, J. Cryst. Growth 318 (2011) 298–303.
[34] A.G. Ostrogorsky, G. Müller, A model of effective segregation coefficient, accounting for convection in the solute layer at the growth interface, J. Cryst. Growth 121 (1992) 587–598.